ACS Catalysis

pubs.acs.org/acscatalysis Research Article

Capturing the Elusive $[Ru^{V}{=}O]^{+}$ Intermediate in Water Oxidation

Daulat Phapale,[‖] Vasudha Sharma,[‖] Abhishek Saini, Sunita Sharma, Pardeep Kumar, Rakesh Kumar, Muralidharan Shanmugam, Apparao Draksharapu, Arnab Dutta,* Eric J. L. McInnes, David Collison, Gopalan Rajaraman,* and Maheswaran Shanmugam*

Cite This: *ACS Catal.* 2024, 14, 11893−11904 Read Online

ACCESS | Metrics & More | Article Recommendations | Supporting Information

ABSTRACT: Although several Ru^{n+} (n = 2 or 3) complexes have been reported to be excellent biomimetics for the water oxidation process of photosystem II, investigation and spectroscopic characterization of the reactive intermediates such as $[Ru^{IV/V}{=}O]^{n+}$ involved in the catalytic process are not only scarce but also a daunting task. Here, we report a catalyst $[Ru^{III}(L)(PPh_3)(H_2O)]^{+}$ (**2**) found to show electrochemical water oxidation efficiency with a considerably low overpotential of 195 mV compared to other Ru^{n+} water oxidation catalysts reported in the nonaqueous media. Besides, the Schiff base ligand (L) employed in this study facilitates the stabilization of a $[LRu^{V}{=}O]^{+}$ species. By the use of multispectroscopic techniques (spectroelectrochemistry, electron paramagnetic resonance, and resonance Raman), we have shed light on the electronic structure of the elusive $[LRu^{V}{=}O]^{+}$ species. Based on the experimental results, a plausible intermolecular radical coupling (I2M) mechanism is proposed, which is corroborated by theoretical calculations.

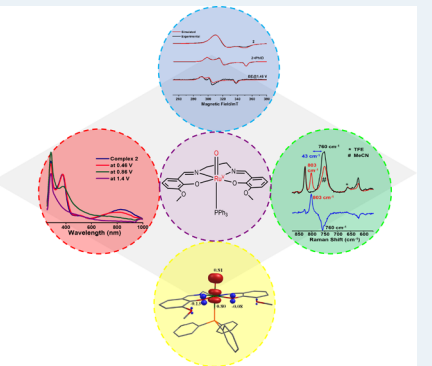

KEYWORDS: *catalysis, water oxidation, ruthenium, high valent metal-oxo, EPR*

INTRODUCTION

Oxidation of water constitutes one of the most challenging processes in artificial photosynthesis, which aims at storing solar energy in the form of chemical bonds of high-energy fuels and is an appealing target reaction for molecular catalysts.[1] The quintessential water oxidation catalysts (WOCs) must possess high efficiency and robustness while operating via a clearly defined mechanism. In the electrochemical water splitting reaction, four electrons/protons along with molecular O_2 are released at the anode (half-cell oxidation reaction) and the released protons get reduced at the cathode (half-cell reduction reaction).[2−5] Compared to the latter, the former reaction (O_2 evolution) is found to be the bottleneck for realizing the "hydrogen economy". Thus, exploiting sustainable sources requires an efficient catalyst, which performs the water oxidation smoothly and efficiently, i.e., comparable to the rate of native photosystem II (PS-II) with a turnover frequency (TOF) of 100−400 s^{-1}.[2−4] After the discovery of the blue dimer, *cis,cis*-$[(bpy)_2(H_2O)Ru^{III}ORu^{III}(OH_2)(bpy)_2]^{4+}$ as a WOC (the first bioinspired model of PS-II), reported by Meyer and co-workers, numerous studies have been undertaken by various researchers to investigate the development of durable and efficient Ru^{n+} catalysts.[6−10] Due to diligent and conscious efforts, not only Ru^{n+} catalysts but also other 3d/4d/5d metal catalysts were identified for this challenging process.[11−15] Nevertheless, the Ru^{n+} catalysts (either a monomer or dimer) show better turnover numbers and TOFs[6,8,14,16−36] than other biomimetic WOCs reported in the literature.[13,37−39] It is evident from the previous reports that either $Ru^{IV}{=}O$ or $Ru^{V}{=}O$ is proposed as an active intermediate for the water oxidation reaction; however, only selected reports provided the spectroscopic and/or structural characteristics of these intermediate species.[40−47] This is largely due to the high reactivity and instability associated with the intermediates. These have been overcome by Lloret-Fillol and co-workers, who managed to crystallize the $Ru^{IV}{=}O$ species and also isolated Ru^{IV}-η^2-peroxo intermediates. These intermediates have been characterized in-depth by resonance Raman (rR), high-resolution mass spectrometry, and isotopic labeling experiments. This particular example strongly supports one of the mechanisms proposed for water oxidation catalysis, i.e., water nucleophilic attack (WNA) on a $Ru^{V}{=}O$ species.[48] The Ru(II) complexes reported by Sun, Llobet, and co-workers and the SCXRD, HR-MS, etc., spectroscopic observations support the other mechanisms for the WOCs, i.e., intermolecular coupling of M^{n+}-oxyl radicals (I2M).[14,32,49−51]

The accelerated reactivity of the ruthenium catalyst presumably hampers the spectroscopic characterization of the

Received: March 16, 2024
Revised: July 13, 2024
Accepted: July 15, 2024
Published: July 25, 2024

https://doi.org/10.1021/acscatal.4c01623
ACS Catal. 2024, 14, 11893−11904

transient species involved in the catalytic process, which is directly evident from the many literature reports.[6,8,14,16,18−26,40,52] The reported catalysts which are efficient and robust consist of pyridyl or polypyridyl ligand platforms with various axial ligands.[14,17−21,40,53,54] Therefore, to intercept the transient species involved in the water oxidation process, the catalyst reactivity should be slowed down drastically so that it will be possible to characterize the transient species via various spectroscopic techniques. For this purpose, one needs to engineer a ligand system that not only acts as an alternate ligand platform (instead of pyridyl or polypyridyl) but also should stabilize the high-valent Ru(IV) and Ru(V) species. In that aspect, the Schiff base ligand emerges as the appropriate choice. Also, it is advantageous that the Schiff base ligand is negatively charged and has strongly σ-donating (less or no π-interaction) character, which may facilitate the access of highly oxidized redox couples $Ru^{V/IV}$ and $Ru^{IV/III}$ at low redox potentials.[19]

Keeping all of these factors in mind, we have utilized the Salen-type Schiff base ligand (H_2L; $C_{18}H_{20}O_4N_2$) to isolate a cationic Ru^{III} complex, with the molecular formula of $[Ru^{III}(L)(PPh_3)(OH_2)]^+$ (**2**). As anticipated, the electrochemical or chemical oxidation of **2** led to the facile access of the transient and high-valent $[LRu^{V}{=}O]^+$ species with a relatively long lifetime of 20−25 min at room temperature. The formation of $[LRu^{V}{=}O]^+$ transient species was thoroughly characterized by spectroelectrochemistry, electron paramagnetic resonance (EPR), and rR-isotopic labeling studies (*vide infra*, Scheme 1). The multispectroscopic

Scheme 1. Various Analytical Techniques and Theoretical Approaches Were Employed for Detecting and Determining the Electronic Structure of the Transient $[LRu^{V}{=}O]^+$ Species, Respectively

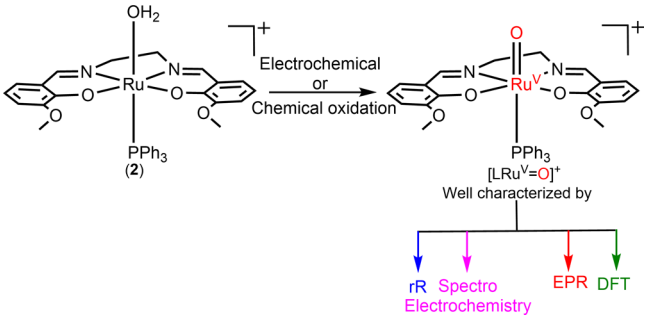

characterization of the high-valent $[LRu^{V}{=}O]^+$ transient species is scarce in the literature due to the extreme reactivity of the transient species. Theoretical calculations were performed not only to support our experimental findings but also to shed light on the electronic structure of the high-valent $[LRu^{V}{=}O]^+$ species formed from **2** (*vide infra*, Scheme 1).

After conducting thorough experimental and theoretical investigations, we present a mechanism for the water-oxidation catalytic cycle. Our findings indicate that the intermolecular radical coupling of $[LRu^{V}{=}O]^+$ (I2M pathway) emerges as the predominant and energetically favorable route for O−O bond formation, surpassing the WNA mechanism (*vide infra*).

RESULTS AND DISCUSSION

The reaction of $[Ru^{III}Cl(L)(PPh_3)]$ (**1**)[55−57] with silver nitrate ($AgNO_3$) and sodium tetraphenylborate ($NaBPh_4$; Scheme S1) yielded green-colored crystals. The data collection and structure solution reveal the molecular formula as $[Ru^{III}(L)(PPh_3)(OH_2)](BPh_4)$ (**2**, Figure 1). In **2**, the dianionic

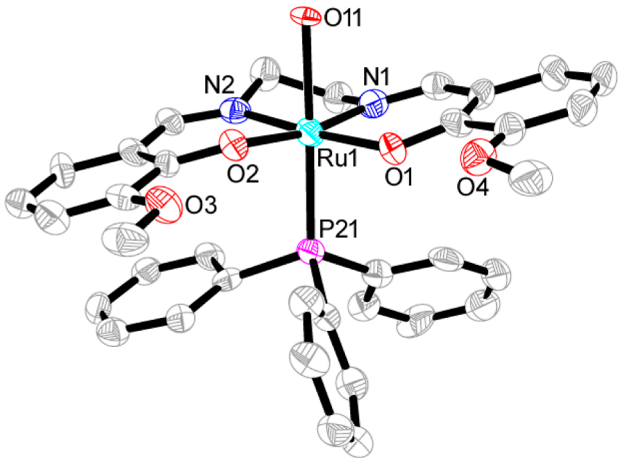

Figure 1. Thermal ellipsoid (50% probability) ORTEP representation of the cationic core of **2**. Cyan = Ru, magenta = P, red = O, blue = N, and gray = C. The hydrogen atoms, solvent molecule, and counteranion (BPh_4^-) were removed for clarity.

tetradentate Schiff base ligand occupies the equatorial plane of octahedral geometry while the axial coordination sites were completed by the water and PPh_3 ligands. The selected bond lengths and angles of **2** are provided in Tables S1−S3. These are consistent with the other Ru^{III} complexes reported in the literature.[55−57] A detailed structural description of **2** is provided in the Supporting Information (Figures S1 and S2). It is noteworthy to mention that ESI-MS data confirmed that the solid-state structure of **2** is maintained in solution as well, where an m/z value of 1027.4467 g/mol is attributed to the $[M + H]^+$ peak.

Significant insight into the redox behavior of **2** is gathered from electrochemical studies performed in dry acetonitrile. All redox potentials reported in this study are against the ferrocenium/ferrocene (Fc^+/Fc) redox couple. The cyclic voltammogram of **2** in dry acetonitrile shows three reversible redox couples at $E_{1/2}$ = −0.57 V, $E_{1/2}$ = 0.51 V, and $E_{1/2}$ = 1.01 V, which are assigned to the metal-based Ru^{III}/Ru^{II}, Ru^{IV}/Ru^{III}, and Ru^{V}/Ru^{IV} redox process (Figure 2A). The control cyclic voltammetry (CV) experiment with the free ligand displayed only an irreversible oxidation signal at 0.80 V (Figure S3). This data strengthen the assignment of metal-based redox couples for **2**. It is noteworthy that the Ru^{V}/Ru^{IV} redox couple is accessed with significantly lower potential than the other Ru^{n+} complexes reported in the literature.[16,53,58,59] A sharp increase in the current is observed at more positive potentials beyond 1.28 V vs Fc^+/Fc, which is attributed to the oxidation of the water molecule that is coordinated to the ruthenium ion in **2** (Figure 2A). Incidentally, we have not only observed a sharp increase in the catalytic current but also the cathodic shift of the Ru(V/IV) redox couple, upon serial addition of water into the mixture. This indicates the possible involvement of the proton-coupled electron transfer (PCET) process (Figure S4).[51] This process is tested by performing the kinetic isotopic experiments using a H_2O and D_2O mixture (H_2O + D_2O = 1 mL). The gradual decrease in the catalytic current observed upon increasing the D_2O concentration in the H_2O/D_2O mixture and the observed k_H/k_D = 1.25 signifies the possible

https://doi.org/10.1021/acscatal.4c01623
ACS Catal. 2024, 14, 11893−11904

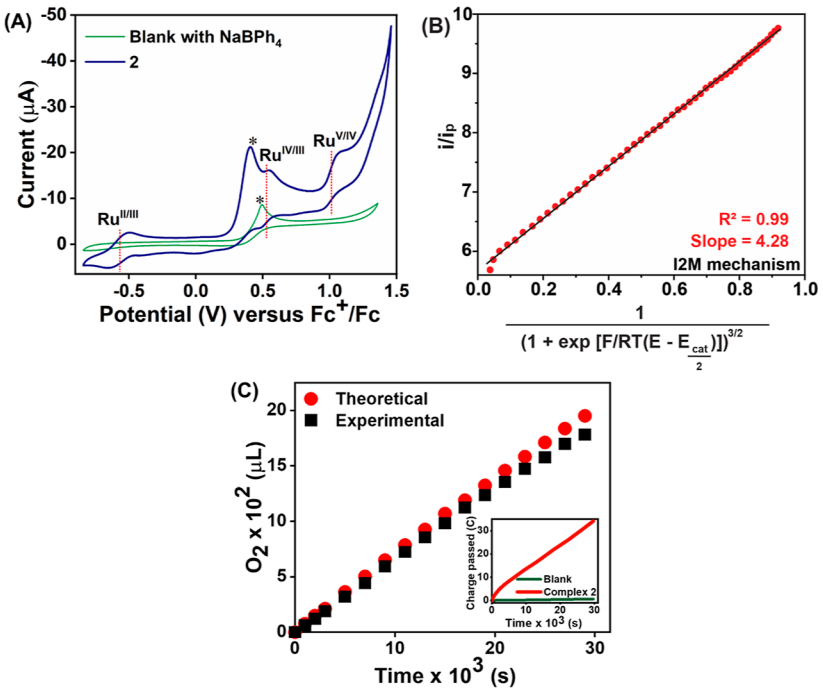

Figure 2. (A) CV of **2** (1.0 mM; blue trace) recorded in dry MeCN solution containing 0.1 M tetrabutylammonium perchlorate at 0.05 V/s scan rate. The green trace and the asterisk mark represent the redox process of the BPh_4^- ion (0.5 mM). (B) Analysis of the catalytic activity **2** by FOWA using the potential−current response from the anodic sweep: 1.04−1.35 V vs Fc^+/Fc. (C) Experimental (black square) and theoretical (red circle) oxygen evolution were observed for **2** (2.5 mM) during a bulk electrolysis experiment performed at 1.46 V vs Fc^+/Fc in the MeCN/H_2O (2:1) mixture under 1 atm N_2 in a closed vessel with a 1 cm × 1 cm reticulated vitreous carbon working electrode at 25 °C. Inset: the charge response during this experiment was recorded for **2** (red trace) and blank solutions (green trace).

involvement of the PCET process that facilitates stabilization of Ru(V/IV) (Figure S5), thus enhancing the catalytic efficiency of **2**. The presence of the strongly σ-donating phosphine, negatively charged Schiff base ligands, and the polar peripheral ether group is likely to support the synchronous proton/electron transfers.[60,61]

To estimate TOF (k_{obs}), variable scan rate measurements (0.1 to 1.0 V/s) were performed with **2** in the presence of an optimal amount of water (300 μL) in acetonitrile (3 mL; Figure S6C). We noticed a 20-fold enhancement in the catalytic current in the presence of water. The constant limiting current is observed when the scan rate is 0.5−1.0 V/s with a diffusion coefficient (D) value of 1.0341×10^{-5} cm^2/s (Figure S6). Under these conditions, the oxidation current recorded for **2** at 1.0 V (vs Fc^+/Fc), which is assigned as $[LRu^V{=}O]^+$ species (*vide infra*), was independent of the scan rate dependency of a stoichiometric redox signal following the Randles−Sevcik equation. A plot of the ratio of catalytic and stoichiometric currents, i.e., i_{cat} to i_p, for the Ru(V/IV) couple as a function of the inverse of the square root of the scan rate is shown in Figure S7. Here, a linear relationship was observed, which is ideally used to estimate the TOF via eq 1 (where i_{cat} is the catalytic current, i_p is the peak current measured in the absence of the substrate (corrected current), n_{cat} is the number of electrons involved in the catalytic reaction, F is Faraday's constant, k_{obs} is the pseudo-first-order rate constant, R is the universal gas constant, T is the temperature in kelvin, and v is the scan rate)

$$\frac{i_{cat}}{i_p} = 2.242 n_{cat} \left(\frac{RTk_{obs}}{F}\right)^{1/2} v^{-1/2} \quad (1)$$

Though Randles−Sevcik equation-derived correlation has been a valuable tool for describing one-electron catalytic processes under ideal conditions, it is challenging to deploy it for complex multielectron processes. Here, a peaked current response was observed during homogeneous catalysis by the Ru complex. Such a response typically indicates that there is a competition between the diffusion of a new substrate to the electrode and its consumption during catalysis. Hence, direct usage of the Randles−Sevcik method for TOF calculation in such conditions can overestimate the TOF and may mask the true kinetic behavior of the system. Hence, the foot-of-the-wave analysis (FOWA) can provide a better picture of the kinetics of this multielectronic oxygen evolving reaction (OER) electrocatalysis driven by **2**. The FOWA is typically represented by eq 2. Here, utilizing the FOWA allows for a more pragmatic analysis, enabling a straightforward determination of kinetic parameters without the complications arising from diffusion limitations and nonlinear effects

$$\frac{i}{i_p} = \frac{4 \times 2.24 \times \sqrt{\frac{RT}{F\nu} k_{obs}}}{\left(1 + e^{F/RT(E - E_{redox})}\right)^x} \quad (2)$$

The FOWA has emerged as an effective method for qualitatively understanding the nature of the WOC mechanism proposed by Costentin and Savéant (eq 2).[62] As proposed earlier, for the WNA or I2M mechanistic pathway, the value of "x" in eq 2 is 1 or 3/2, respectively.[62−64] The rate [k_{obs} (or TOF)] of the reaction was calculated from the slope of the linear plot obtained between $\frac{i}{i_p}$ and $\frac{1}{(1 + e^{F/RT(E - E_{cat/2})})^x}$. Here, the experimentally measured $\frac{i}{i_p}$ values were plotted against

https://doi.org/10.1021/acscatal.4c01623
ACS Catal. 2024, 14, 11893−11904

$\frac{1}{(1+e^{F/RT(E-E_{cat/2})})^x}$ with both the possible values of $x = 1$ and $x = 3/2$, and better linearity is observed for $x = 3/2$ (Figures 2B and S8) compared to when $x = 1$ (Figure S8) and the rate of the reaction estimated from the slope of the linear fit of FOWA yields 0.44 (±0.02) s^{-1}. Hence, this analysis suggests that **2**-catalyzed water oxidation likely follows an I2M pathway. This is in good agreement with the other experimental observations (rR and EPR) which are further corroborated by the computational study (*vide infra*).

We have also recorded the blank Pt electrode background response for the OER after adding different amounts of water (Figure S9A), where we noticed only a minimal contribution for the background OER activity (20 μA current with a slanted slope) compared to the same in the presence of **2** (150 μA current with a stiff slope). This observation indicates a distinct catalytic response in the presence of **2** beyond 1.1 V (Figure S9B).

Further analysis suggested that **2** catalyzes water oxidation with an overpotential of 195 mV (onset potential = 1.28 V, $E_{cat/2}$ = 1.405 V; Figure S10), which is significantly lower than other WOCs reported in the nonaqueous medium (MeCN),[65] while it is comparable to the overpotential, reported for certain ruthenium catalysts in aqueous media.[60,66] Although the ruthenium complex is not soluble in aqueous solutions, we made efforts to evaluate its potential for water oxidation utilizing Britton−Robinson universal buffer across a range of pH values (2−14, refer to Figure S11; 33% v/v) in acetonitrile solvent (2:1 ratio). Among the pH conditions explored, pH 8 emerged as optimal for water oxidation efficiency, surpassing other pH ranges (Figure S11). Therefore, to evaluate the OER efficiency of the complex via bulk electrolysis, we have maintained the same solvent ratio (2:1) with **2** dissolved in MeCN and pure water added. The amount of O_2 evolved was calculated from bulk electrolysis of **2** in the MeCN/H_2O mixture (15 mL, 2:1 ratio (v/v); Figure 2C). After 500 min of continuous electrolysis at 1.46 V (vs Fc^+/Fc), passing of 33.6 C was recorded along with the production of 79.5 μmol of O_2, corresponding to a Faradaic efficiency (FE) of 91.3% (see the Supporting Information for the Faradaic efficiency calculation section). To investigate the homogeneous nature of **2** in this catalysis process, we conducted a series of tests. First, we performed a rinse test during the electrochemical reaction. Subsequently, we analyzed the system using dynamic light scattering and scanning electron microscopy before and after bulk electrolysis. Our findings (see the Supporting Information for details and Figures S12−S14) indicate that there was no nanoparticle deposition observed on the active surface area of the working electrode. This suggests that **2** maintained its homogeneity throughout the catalytic process.

Next, we turned our focus to identifying the nature of the transient species responsible for water oxidation. DPV experiments were performed in DMF to avoid the MeCN evaporation that exhibits similar redox processes as those observed in MeCN (Figure S15). For this, initially, we performed detailed spectroelectrochemistry experiments (Figures S16−S18). The absorption spectrum of **2** shows intense bands in the region of 200−400 nm (ε = 75940 M^{-1} cm^{-1}) which are attributed to the ligand-based ($\pi-\pi^*$) charge transfer along with a broad band observed in the 600−1000 nm region, which is assigned to the metal to ligand charge transfer (MLCT) transition. The band's assignment was also consistent with the TD-DFT calculations performed on this complex (*vide infra*). It is unusual to see absorption bands of such intensity around 820 nm (ε = 20, 100 M^{-1} cm^{-1}) for Ru(III) complexes.[67] A spectroelectrochemical experiment was performed on **2** at applied potential values of 0.46, 0.86, and 1.4 V (vs Fc^+/Fc), and the corresponding changes in the visible and NIR regions were monitored (Figure 3). The

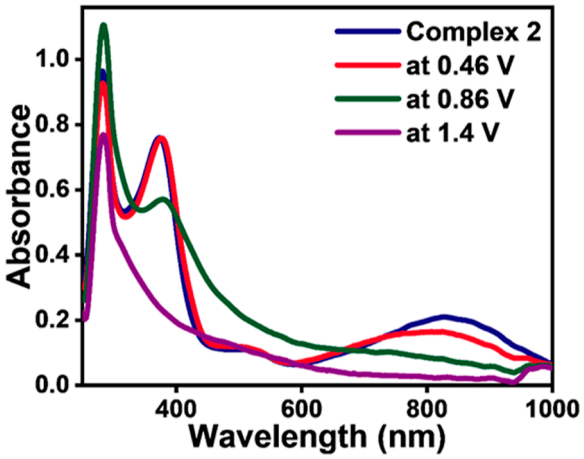

Figure 3. Spectroelectrochemical UV/vis/NIR spectral changes in **2** (1×10^{-5} M) observed upon the applied potentials of 0.46 V (red trace), 0.86 V (green trace), and 1.4 V (purple trace) vs Fc^+/Fc in DMF at room temperature.

MLCT as well as ligand-centered bands are directly influenced by the Ru^{IV}/Ru^{III} (at 0.46 V) and Ru^{V}/Ru^{IV} oxidation (0.86 and 1.4 V), i.e., the intensity of those bands gradually decreases and finally disappears as a function of increasing applied potential (Figure 3). This is consistent with the sequential removal of electrons from the Ru^{III} ion in **2** ($Ru^{III} \rightarrow Ru^{IV} \rightarrow Ru^{V}$), i.e., the insufficient electron density on the metal center leads to weaker and/or no charge-transfer transition. A similar scenario has been witnessed for other Ru-based WOCs reported in the literature.[23,61] Hence, the cyclic voltammetric and spectroelectrochemistry studies support the formation of high-valent Ru species from **2** during the bulk electrolysis responsible for water oxidation.

Before we intend to intercept the electrochemically/chemically generated reactive Ru^{V} species, the electronic structure of **2** was investigated (in both solid state and frozen solution) by X-band (9.384 GHz) cw-EPR measurements at low temperature. The EPR spectra of a polycrystalline powder and its frozen MeCN solution of **2** are detailed in the Supporting Information. In both cases, **2** shows a rhombic signal[68] (refer to Figures S19 and S20 of the Supporting Information).

To reinforce the evidence of the disappearance of MLCT at 1.4 V, attributed to the emergence of Ru(V) species in spectroelectrochemical experiments, we reproduced the generation of these species through bulk electrolysis which was carried out in a MeCN/H_2O mixture by holding the potential at 1.46 V at room temperature. At this potential, we have shown above that 79.5 μmol of O_2 (Figure 2C) liberates upon water oxidation after the elusive Ru(V) species formation. The species so generated through the bulk electrolysis exhibited notably distinct EPR spectral features compared to pure **2** (see the Supporting Information for methods and sample preparation). The rhombic EPR signal observed at X-band (ν = 9.106 GHz) frequency for the species

https://doi.org/10.1021/acscatal.4c01623
ACS Catal. 2024, 14, 11893−11904

is consistent with S = 1/2 and has g-values = [1.920 2.143 2.245] (Figure 4). The extracted spin Hamiltonian parameters

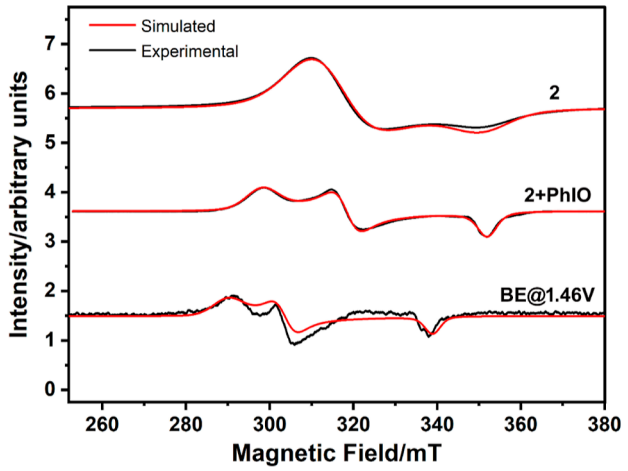

Figure 4. Frozen solution X-band EPR spectrum of **2** (top trace). The cw-EPR spectra of the transient species generated from **2** upon treating with PhIO (middle trace) or electrochemically via bulk electrolysis (BE @ 1.46 V; bottom trace); *experimental conditions* with temperature = 20 K; MW frequency = 9.384 GHz for **2** and **2** + PhIO as frozen solutions in MeCN (20 K) and 9.106 GHz at 77 K for BE@ 1.46 V in MeCN/H_2O (2:1) mixture.

are attributed to the formation of the transient Ru^V species [Ru^{IV} usually has an integer electron spin (S = 1) with a large D (zero-field splitting) value, which is expected to be EPR silent]. Upon increasing the concentration of **2** from 0.5 to 2.5 mM during bulk electrolysis, the EPR spectral features for the transient Ru(V) that was observed earlier at low concentration are not observed. This indicates that the lifetime of Ru(V) is dictated by the concentration of this species formed, which might give insights into the nature of the mechanism involved in water oxidation catalysis (*vide infra*).

To provide evidence for the generation of elusive Ru^V from **2** chemically, EPR spectra were recorded for **2** in MeCN in the presence of the two-electron oxidizing agent iodosyl benzene (PhIO) (1:6 ratio of **2** and PhIO; Figures 4 and S21).[69,70] It is evident from the comparison of the EPR spectra of **2** and **2** + PhIO that new EPR signals are formed, which are successfully simulated with the following spin-Hamiltonian parameters; g = [1.905 2.106 2.249]; Voigtian broadening = [2.9 1.9] mT; and HStrain = [0 102 208] MHz, again consistent with S = 1/2 Ru^V species. The g-values observed for the electrochemically generated and chemically generated Ru^V species are similar but not identical, however, distinctly different from **2**. This experiment further enables us not only to affirm the formation of Ru(V) species but also to carry out the isotopic labeling experiments to substantiate the evanescent terminal $[Ru(V)=O]^+$ species through rR (*vide infra*).

The electrochemical, spectroelectrochemistry, and EPR measurements confirm the formation of Ru^V species from **2**. However, the specific structure pertaining to the Ru^V transient intermediate remains undisclosed, and the major difficulty arises in discerning the existence of a terminal oxo ligand attached to the central ruthenium ion. rR studies were conducted at room temperature to elucidate the existence of terminal oxo Ru(V) species in the solution. The rR spectrum of **2** in acetonitrile with λ_{exc} at 405 nm results in the enhancement of bands at 1602, 1536, 1414, 1365, 1345, 1300, 850, 732, and 615 cm^{-1} (Figure S22). These bands are tentatively assigned to the phenolic and imine groups present in L^{2-} of **2**.

Reacting **2** with 6 equiv of PhIO in CH_3CN in the presence of a minuscule amount of water (20 μL, 1.1 M) at room temperature shows resonantly enhanced bands at 803 and 615 cm^{-1} (Figure 5B). The intensity of the 803 cm^{-1} band decreases over 25 min, with a concomitant increase in the intensity of the band at 615 cm^{-1} (Figure 5B). Therefore, the peak observed at 803 cm^{-1} is attributed to the transient species formed from **2** in the presence of PhIO (Figure 5). This 803 cm^{-1} peak shifted to 760 cm^{-1} upon treatment of **2** with ^{18}O-labeled PhIO while the 615 cm^{-1} band remained unaffected (Figure 5A).

The observed 43 cm^{-1} shift is in the expected range for either the terminal Ru^V=O (41 cm^{-1}) or O−O (48 cm^{-1}) oscillator following Hooke's law.[42,71,72] To unambiguously determine this aspect, we have generated the transient species by reacting **2** with an equimolar mixture of $PhI^{16}O$ and $PhI^{18}O$

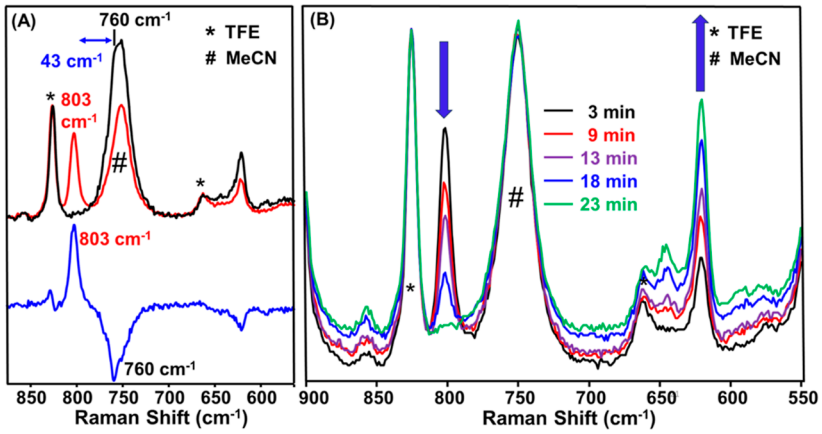

Figure 5. (A) rR spectra at λ_{exc} 638 nm of $[LRu^V=O]^+$ generated by using $PhI^{16}O$ (red trace) and $PhI^{18}O$ (black trace) from **2** in MeCN at room temperature. The difference spectrum shows 803 cm^{-1} as positive and 760 cm^{-1} as the negative band (blue trace). Condition to generate $[LRu^V=O]^+$: 0.3 mM **2** in MeCN + 10 equiv PhIO or $PhI^{18}O$ in trifluoroethanol (TFE). (B) The self-decay of the intermediate ($[LRu=O]^+$) (generated by the reaction of 0.3 mM **2** in MeCN and 10 equiv PhIO in TFE) was followed by rR spectroscopy at room temperature. # indicates peak from the CH_3CN solvent, and * indicates peak from the TFE solvent.

https://doi.org/10.1021/acscatal.4c01623
ACS Catal. 2024, 14, 11893−11904

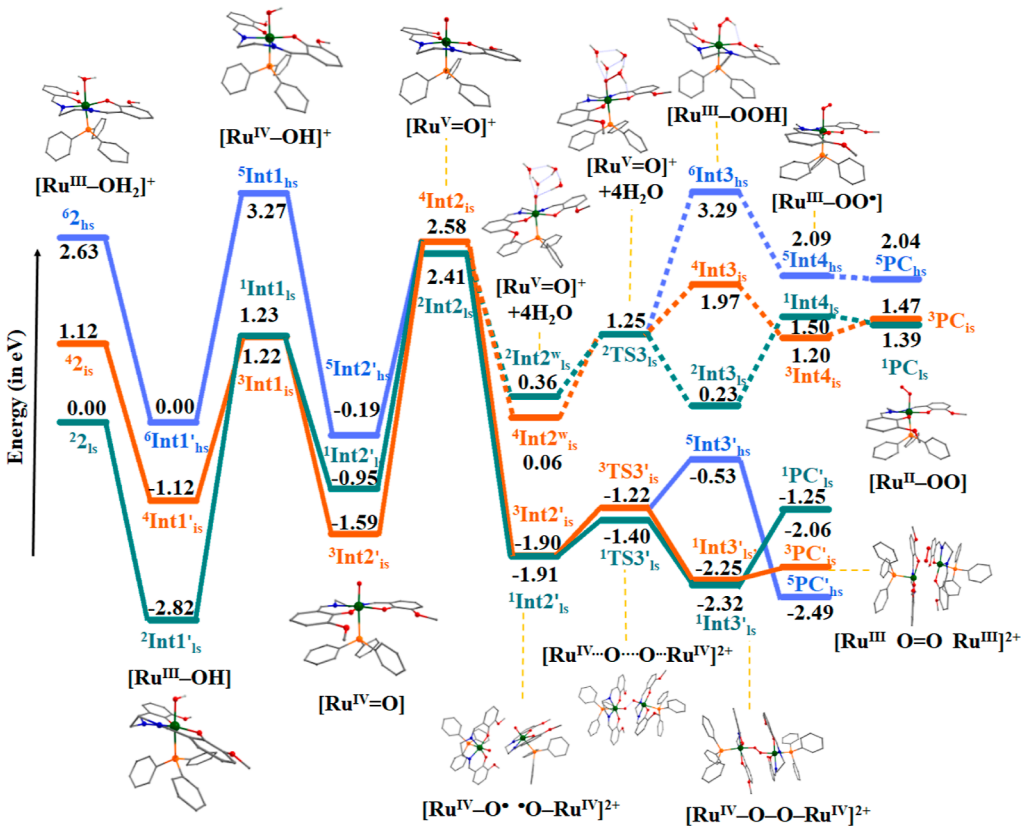

Figure 6. Energy profile diagram for the proposed mechanism, containing solvent-free energies (ΔG), for the water oxidation process proceeding by **2**. Here, the dotted line represents the WNA mechanism and solid line represents the I2M mechanism.

(overall 10 equiv), which exhibits again bands at 803 and 760 cm^{-1}. The absence of a band at ca. 780 cm^{-1} (expected from the $^{16}O-^{18}O$ oscillator) suggests that the 803 cm^{-1} band indeed originates from a terminal $Ru^{V}{=}O$ species (Figure S23).

In addition, an 803 cm^{-1} band was also observed when **2** was reacted with 10 equiv PhIO in 1:1 CH_3CN/H_2O (v/v), indicating that the existence of the same intermediate during the water oxidation process is feasible (Figure S24). To our surprise, the decay rate of the intermediate is unaffected in the presence of H_2O or D_2O (Figures S25 and S26), indicating that the WNA of $[LRu^{V}{=}O]^{+}$ is not that facile. At the same time, the unchanged decay rate (even in the presence or absence of H_2O/D_2O) implies that the intermolecular radical coupling mechanism of $[LRu^{V}{=}O]^{+}$ appears to be favored. This mechanism is further strongly supported by the observation of a strong increase in the current beyond 1.28 V vs $Fc^{+/0}$ in the cyclic voltammogram of **2** in dry acetonitrile (due to the catalytic water oxidation; refer to Figure 2A), i.e., in the absence of added external water. The 20-fold increase in current upon the addition of the optimum amount of water (300 μL) in the CV experiment presumably reinstates the formation of **2** (Figure S6C) and the catalytic cycle continues.

To further corroborate the I2M mechanism, concentration-dependent rates of decay studies were performed on the $[LRu^{V}{=}O]^{+}$. We recorded rR data at λ_{exc} = 638 nm using varying concentrations (0.3, 0.6, and 0.9 mM) of **2** with 10 equiv of PhIO. Following the intensity of the 803 cm^{-1} band as a function of time (normalized with respect to the 825 cm^{-1} peak from the TFE solvent) allowed us to determine the observed rate constant (k_{obs}) at each concentration. However, we encountered a practical challenge at higher concentrations, where the decay of intermediate $[LRu^{V}{=}O]^{+}$ was exceptionally rapid (e.g., at 0.9 mM, decaying within 4 min; see Figures S25−S28 in the Supporting Information). As the kinetics were monitored using rR, it was not feasible to obtain a sufficient number of data points for reliable fitting due to the rapid decay of the $[LRu^{V}{=}O]^{+}$ species. The absence of EPR signals for the electrochemically generated transient Ru(V) at a higher concentration (2.5 mM) again reiterates the fact that the radical coupling mechanism is favored over the WNA of Ru(V) species in water oxidation catalysis. Theoretical calculations are also consistent with our experimental observation (*vide infra*).

DFT calculations were carried out to understand the detailed mechanistic insights of the catalytic activity of **2** and the role of a $[LRu^{V}{=}O]^{+}$ intermediate species (see the Supporting Information). Among three possible spin states, the reactant was found to have a doublet ground state ($^{2}\mathbf{2}_{ls}$) with $(d_{xz})^2(d_{xy})^2(d_{yz})^1(d_{z^2})^0(d_{x^2-y^2})^0$ electronic configuration [quartet ($^{4}\mathbf{2}_{is}$) and sextet ($^{6}\mathbf{2}_{hs}$) states lie at 1.12 and 2.63 eV, respectively (Figures S29−S31 and Tables S5 and S6)]. The computed TD-DFT plot for the $^{2}\mathbf{2}_{ls}$ state is in good agreement with the experimental data, offering further confidence in the computational methodology employed (see Figures S32 and S33). Additionally, the computed EPR values for the ground state ($^{2}\mathbf{2}_{ls}$), **g** = [1.967 2.127 2.178], are in good agreement with the experimentally extracted g-matrix, further validating our computational findings (Table S7). In the subsequent step of the proposed mechanism of water splitting, the constructed thermodynamic cycle (see Figures 6 and S34) suggests that the reaction proceeds favorably via the proton transfer (PT)−electron transfer (ET) pathway for the O−H bond activation

https://doi.org/10.1021/acscatal.4c01623
ACS Catal. 2024, 14, 11893−11904

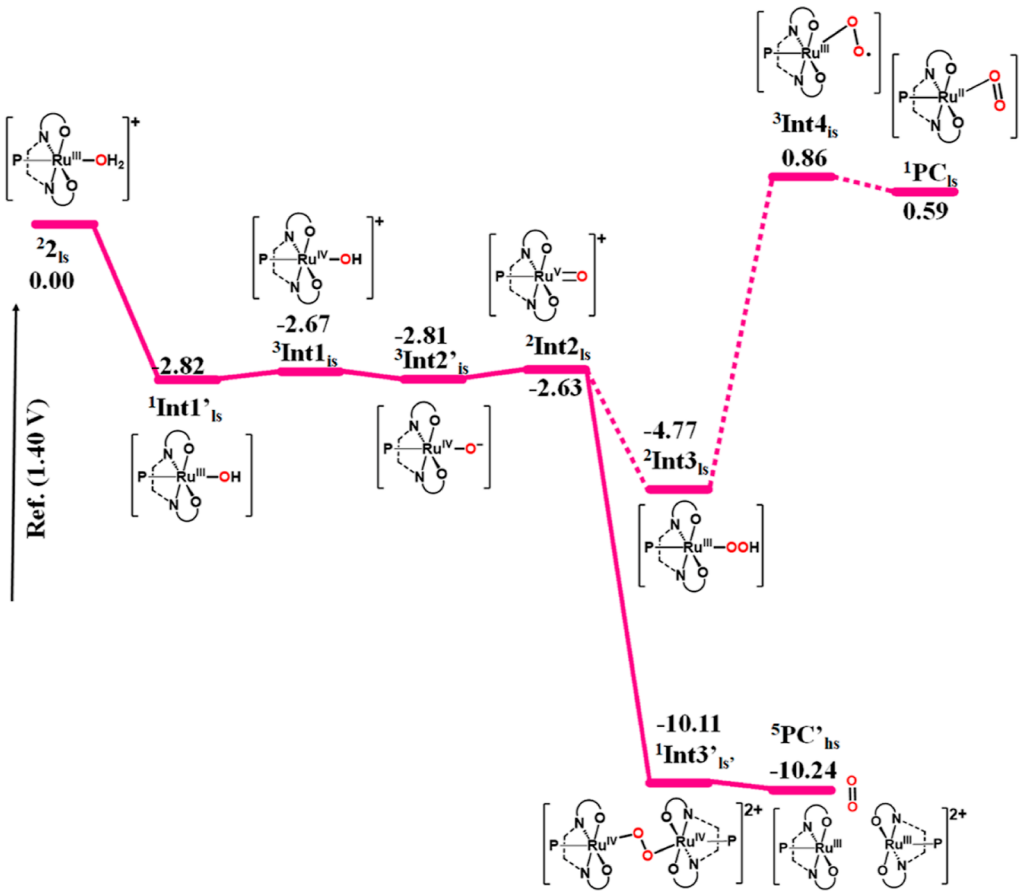

Figure 7. Energy profile diagram for the proposed mechanism with respect to the redox potential (in eV, see the Computational Detail section), for the water oxidation reaction proceeding by **2**. Here, the dotted line represents the WNA mechanism and solid line represents the I2M mechanism.

among the tested pathways. The formation of a $[Ru^{III}-OH]$ intermediate (^{2}**Int1′**$_{ls}$) is found to be exothermic by −2.82 eV and the follow-up $[Ru^{IV}-OH]^{+}$ species has an energy penalty of 1.22 eV (^{3}**Int1**$_{is}$) (see Figures 6 and S34).

Although the formation of $[Ru^{IV}-OH]^{+}$ appears to be significantly endothermic, it is important to note here that this energy is computed without any reference point. If the entire potential energy surface is reconstructed using the experimental potential of 1.40 V, all of the steps computed were found to be exothermic (see Figure 7). The $[Ru^{III}-OH]$ to $[Ru^{IV}-OH]^{+}$ conversion in this reference potential is found to be +0.15 eV, suggesting a favorable process if the external potential is taken into consideration. A very strong $[Ru^{III}-OH]$ bond with a significant π-donation from the −OH group stabilizes this species as shown in the NBO analysis (1.58 eV in second-order PT analysis, see Figure S35), and this is evident from a short Ru−O(H) distance of 1.970 Å, which is ∼0.331 Å shorter compared to the reactant complex leading to the exothermic formation. However, in the following electron transfer process, the Ru^{III} metal is oxidized to Ru^{IV}, which is unfavorable for the given ligand environment (Figures S36−S39).[73] The computed redox potential, while going from ^{2}**2**$_{ls}$ $[Ru^{III}-OH_2]^{+}$ species to $[Ru^{IV}-OH]^{+}$ species (^{3}**Int1**$_{is}$), closely matches the experimental observations, with a value of 0.56 V (Table S8).

The thermodynamic cycle suggests that the next step of the mechanistic pathways proceeds via the PT−ET pathway wherein the $[Ru^{IV}-OH]^{+}$ (^{3}**Int1**$_{is}$) species converts into $[Ru^{V}=O]^{+}$ (^{2}**Int2**$_{ls}$) species (Figures S40 and S41). The PT−ET step has energy margins of −1.59 and 2.41 eV, respectively. In the case of PT, the geometrical change of the attached ligand from −OH to $-O^{2-}$ (in the species $[Ru^{IV}-OH]^{+}$ to $[Ru^{IV}=O](^{3}$**Int2′**$_{is})$) leads to $Ru^{IV}=O$ wherein the oxide makes a π-bond to stabilize Ru in the +4 oxidation state, compared to the −OH counterpart where only a partial π-bond was detected [WBI index value is 0.77 vs 1.28 (Table S9), Figure S42]. This π-bond facilitates the further formation of the putative $[Ru^{V}=O]^{+}$ species, though this step is endothermic, as expected (see the Supporting Information). The $Ru^{V}=O$ species has two different spin states, namely, S = 3/2 and S = 1/2, the doublet computed to be the ground state (2.41 eV; see Figure 6), agrees with the cw-EPR measurement performed for $[Ru^{V}=O]^{+}$ species (S = 1/2). For the doublet ground state, not only is the computed $[Ru^{V}=O]^{+}$ vibration (789.3 cm^{-1}) in good agreement with the experiment (803 cm^{-1}) but also the computed absorption features for ^{2}**Int2**$_{ls}$ (Figure S43) match well with spectroelectrochemical measurements. Furthermore, the $[Ru^{V}=O]^{+}$ bond distance is computed to be 1.779 Å which is in good agreement with the previous reports (1.700−1.760 Å).[74,75] In order to further validate the formal oxidation state of the Ru ion in **Int2** species, we have performed the rigid scan by varying the Ru−O distance from 1.778 to 1.998 Å. Our computational findings suggest that as we transition from $Ru^{V}=O$ to $Ru^{IV}-O^{\bullet}$, the radical character on oxygen strengthens, while the spin density on Ru slightly decreases. Additionally, with an increase in the bond length, the Ru−O bond stretching frequency notably decreases, falling below ∼750 cm^{-1}, which further supports the

https://doi.org/10.1021/acscatal.4c01623
ACS Catal. 2024, 14, 11893−11904

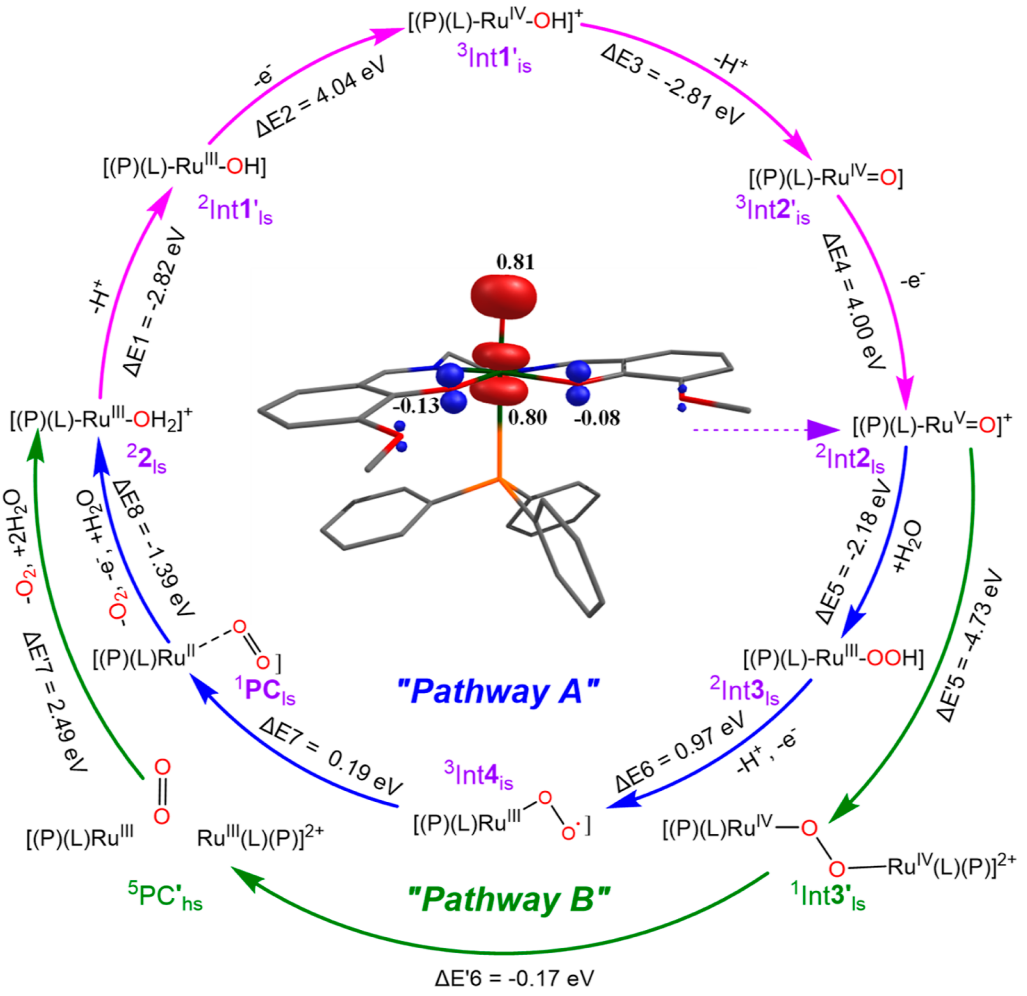

Figure 8. Proposed mechanistic pathway of the water oxidation reaction proceeding by **2** via WNA (pathway A) and I2M (pathway B) mechanisms. Inset: The spin density plot given corresponds to $[(P)(L)\text{-}Ru^{V}{=}O]^{+}$ species. In this scheme, P and L represent the PPh_3 and doubly deprotonated Schiff base ligand ($C_{18}H_{20}O_4N_2$).

oxidation state being +5. Moreover, the formation of a genuine $Ru^{IV}{-}O^{\bullet}$ entity is also significantly endothermic (41.8 kJ/mol), discouraging the formation of such species (Figure S44).

A spin density plot reveals strong delocalization of electrons from Ru to the oxo center with significant spin polarization (negative spin density) detected in the ligand framework (for NBO analysis, see Figure S45). Since the net spin density detected in the {Ru−O} fragment is ∼1.61, the additional gain in electron was obtained via spin polarization of the ligand, suggesting $L^{\bullet\downarrow}{-}Ru^{V\uparrow}{-}O^{\bullet\uparrow}$-type ground state structure, unveiling the importance of the redox active Schiff base ligand in stabilizing such a high-valent species. To affirm this further, we have now performed spin natural orbital analysis, which clearly shows three electrons in the Ru center, suggesting a +5 oxidation state (Figure S46) (see the inset of Figure 8 for spin density.) In the proceeding step, $[Ru^{V}{=}O]^{+}$ or $L^{\bullet\downarrow}{-}Ru^{V\uparrow}{-}O^{\bullet\uparrow}$ species perform the OER, and here, we have considered two probable mechanisms: (i) WNA mechanism leading to the formation of the O−O bond and Ru^{III}−OOH species (see Figures 6 and 8) and (ii) I2M mechanism leading to the formation of end-on $[Ru^{IV}{-}O{-}O{-}Ru^{IV}]^{2+}$ species.[35] The computed potential energy surface considering both WNA and I2M mechanisms is shown in Figure 6.

To understand the kinetic requirement of this process further, the transition state (^{2}**TS3**$_{ls}$) has been calculated for the O···O bond formation step from ^{4}**Int2**$^{w}_{is}$, and four water molecules yielded a barrier of 1.25 eV from a reactant complex (Figure S47). Given that $[Ru^{V}{=}O]^{+}$ formation itself is energy demanding, the WNA mechanism requires further energy for the O···O bond formation (Figures S48−S50) for species ^{2}**Int3**$_{ls}$, ^{3}**Int4**$_{is}$, and ^{1}**PC**$_{ls}$, and therefore, it can be ruled out. In the I2M mechanism, two molecules of $[Ru^{V}{=}O]^{+}$ are expected to approach each other, resulting in the formation of a singlet dimer species (^{1}**Int2′**$_{ls}$), with an expected spin density pattern of $[Ru^{IV\uparrow}{-}O^{\uparrow}O^{\downarrow}{-}Ru^{IV\downarrow}]^{2+}$ at the transition state (see Figure S51). Such a mechanism with lower kinetic barrier at the open-shell singlet has been proposed earlier by Privalov and co-workers for the O_2 evolution reaction involving a seven coordinate Ru species.[14] This process is computed to be exothermic with an energy margin of −1.91 eV, indicating the thermodynamic favorability of this pathway. During the formation of this dimer species (^{1}**Int2′**$_{ls}$), the O···O distance is found at 4.812 Å, which subsequently decreases to 1.882 Å during the formation of the O−O coupling transition state (^{1}**TS3′**$_{ls}$) (Figure S52). This singlet transition state shows spin density as $\{O_{(0.67)}\cdots O_{(-0.61)}\}$ during the transition state, which facilitates the formation of the O−O bond. The spin density pattern at the oxygen is the same as we have anticipated. The energy gap between the ^{1}**Int2′**$_{ls}$ state and the ^{1}**TS3′**$_{ls}$ state is found to be 0.51 eV, which is notably lower

https://doi.org/10.1021/acscatal.4c01623
ACS Catal. 2024, 14, 11893−11904

than the transition state energy barrier in the WNA pathway (1.25 eV). These computational results suggest that the bimolecular pathway is more favorable compared with the WNA pathway. Subsequently, this dimerization transition state leads to the formation of $[Ru^{IV}-O-O-Ru^{IV}]^{2+}$ (Figure S52). The formation of the $[Ru^{IV}-O-O-Ru^{IV}]^{2+}$ species is found to be even more exothermic, with an energy release of −2.32 eV. Furthermore, there are several strong C−H.π interactions as well as the $\pi-\pi$ interactions (as confirmed by AIM analysis, Figures S53 and S54) between both L in the two Ru-oxo species that were found to stabilize such a dimeric species. Among the various spin states calculated, the singlet ground state ($S = 0$) was found to be the ground state of the dimeric species. The Ru−O distance was found to be 1.967 Å and the O−O distance was found to be 1.345 Å, and this is consistent with the similar end-on peroxo species reported earlier.[22] The $\nu_{(O-O)}$ stretching frequency is 667.3 cm^{-1}, which matches a feature observed at 645 cm^{-1} in the rR experiments.

This is aided by significantly longer Ru−O distance and a partial triplet character already developed at the ground-state structure (Figures S55 and S56). An exothermic step by 0.17 eV leads to the facile formation of oxygen once $[Ru^{V}=O]^{+}$ formation takes place. The O−O bond distance at the product complex is computed to be 1.214 Å, which is similar to that found in O_2, suggesting a favorable release of O_2 compared to the WNA mechanism, which has a steeper energy penalty (Figure 6). During the formation of the product complex, Ru^{IV} converts to Ru^{III} and the presence of a water molecule regenerates **2** and the catalytic cycle continues. Thus, energetics supports the mechanism of the OER via the I2M pathway and not the WNA pathway (Figures S51−S65). A large energy penalty associated with the nucleophilic attack of H_2O on the oxo atom leading to the $Ru^{III}-OOH$ species was found to be the differentiator and absence of functional groups in the ligand framework that can anchor water in the vicinity of the $Ru^{V}=O$. Both of these factors facilitate the formation of $[Ru^{IV}-O-O-Ru^{IV}]^{2+}$ species and thus the I2M pathway is dominant over WNA. In rR studies, the observation that $[Ru^{V}=O]^{+}$ in the presence of water does not decay faster than the self-decay strongly suggests a significant energy penalty for the nucleophilic attack, along with a weak feature observed at 645 cm^{-1} that grows with the decay of $[Ru^{V}=O]^{+}$ species in the rR experiments and might indicate I2M mechanism, but we cannot conclusively state this as this peak is insensitive to ^{18}O-labeling studies.

The mechanism for the water oxidation catalyzed by **2** is provided based on the results of electrochemical data, rR, EPR, and theoretical studies (Figure 8). The proposed mechanism is in line with the mechanism explored for monometallic $Ru^{(II)/(III)}$ complexes in the literature.[14,16−23,40,52−54,58,76,77] The initial two steps of the catalysis involve the loss of $2e^{-}$ and $2H^{+}$ resulting in the formation of the $[LRu^{V}=O]^{+}$ intermediate from the parent **2**. Considering that the rate of decay of $[LRu^{V}=O]^{+}$ is independent of H_2O/D_2O in rR measurements and the rate of decay of this transient species depends on the concentration of **2** (also observed in cw-EPR measurements) suggests that the I2M mechanism is a more favorable pathway (pathway B in Figure 8) than the WNA mechanistic pathway. Following this, O_2 evolution and regeneration of **2** is found to be the facile pathway in the presence of water, thus the catalytic cycle continues. Based on our results, we have made a qualitative comparison (Table S10 and Figure S66), which indicates that when the overall charge on the coordination sphere of $[Ru^{V}=O]$ is ≤+1, an I2M mechanism is favored. Conversely, when the overall charge exceeds +1, the WNA mechanism predominates. For example, like in our case, Sun et al. have documented the presence of a $[Ru(V)=O]^{+}$ species, which favors the I2M mechanism,[49] whereas Meyer et al. have found the presence of a $[Ru(V)=O]^{3+}$ species that facilitates the WNA pathway.[16,53] This trend illustrates that by modulation of the charge of the anchoring ligand, the overall water oxidation mechanism can be modulated, which will eventually be useful in designing efficient catalysts for water oxidation.

CONCLUSIONS

The reaction of preformed Ru(III) precursor complex **1** with $AgNO_3$ and $NaBPh_4$ led us to isolate **2**. The structure of **2** was elucidated by single-crystal X-ray diffraction. The presence of a negatively charged Schiff base ligand and a strong σ-donating phosphine ligand around the Ru^{III} center facilitates access to the higher oxidation states (Ru^{IV} and Ru^{V}) at considerably lower potentials. Also, the involvement of the PCET process, which prevents the high charge accumulation around the metal center, provides additional stability to the transient species. The electrochemical and spectroelectrochemical investigations disclose that $[LRu^{V}=O]^{+}$ is involved in catalytic water oxidation. The formation of $[LRu^{V}=O]^{+}$ was unambiguously confirmed by the EPR and rR studies. The electronic structure of the transient $[LRu^{V}=O]^{+}$ species (generated both chemically (PhIO) and by bulk electrolysis) is confirmed by the variable-temperature X-band EPR spectroscopy. The energetics and stretching frequencies computed for the various intermediates are in line with experimental observations, further strengthening the involvement of $[LRu^{V}=O]^{+}$ species in the water oxidation. All these experimental and theoretical studies suggest that the I2M mechanism is more favorable than the WNA mechanism. The transient species $[LRu^{V}=O]^{+}$ that was characterized by various analytical techniques provides a further understanding of the species involved in the catalytic cycle. Attempts to isolate/characterize the peroxo-bound ruthenium intermediates are currently in progress, which will eventually help us to understand the mechanism even better and to design more efficient WOCs.

ASSOCIATED CONTENT

Supporting Information

The Supporting Information is available free of charge at https://pubs.acs.org/doi/10.1021/acscatal.4c01623.

Instructions, experimental procedures, structural details and packing diagram of **2**, CV, LSV plots at various scan rates, isotope kinetic study plots, EPR spectra of both **2** and **2**+ PhIO at various temperatures (both polycrystalline and frozen samples), detailed resonance Raman studies of **2** and **2**+PhIO (H_2O^{18}-labeling studies and concentration-dependent studies), spectroelectrochemical absorbance studies at various potentials, and computational results (PDF)

CCDC number for **2**: 2352455 (CIF)

AUTHOR INFORMATION

Corresponding Authors

Arnab Dutta − *Department of Chemistry, Indian Institute of Technology Bombay, Mumbai 400076 Maharashtra, India*; Email: arnabdutta.iitb@gmail.com

https://doi.org/10.1021/acscatal.4c01623
ACS Catal. 2024, 14, 11893−11904

Gopalan Rajaraman − *Department of Chemistry, Indian Institute of Technology Bombay, Mumbai 400076 Maharashtra, India;* orcid.org/0000-0001-6133-3026; Email: gopalan.rajaraman@gmail.com

Maheswaran Shanmugam − *Department of Chemistry, Indian Institute of Technology Bombay, Mumbai 400076 Maharashtra, India;* orcid.org/0000-0002-9012-743X; Email: eswar@chem.iitb.ac.in

Authors

Daulat Phapale − *Department of Chemistry, Indian Institute of Technology Bombay, Mumbai 400076 Maharashtra, India*

Vasudha Sharma − *Department of Chemistry, Indian Institute of Technology Bombay, Mumbai 400076 Maharashtra, India*

Abhishek Saini − *Department of Chemistry, Indian Institute of Technology Bombay, Mumbai 400076 Maharashtra, India*

Sunita Sharma − *Department of Chemistry, Indian Institute of Technology Bombay, Mumbai 400076 Maharashtra, India*

Pardeep Kumar − *Department of Chemistry, Indian Institute of Technology Bombay, Mumbai 400076 Maharashtra, India*

Rakesh Kumar − *Department of Chemistry, Indian Institute of Technology Kanpur, Kanpur 208016 Uttar Pradesh, India*

Muralidharan Shanmugam − *Department of Chemistry and Photon Science Institute, The University of Manchester, Manchester M13 9PL, U.K.;* orcid.org/0000-0003-3818-1401

Apparao Draksharapu − *Department of Chemistry, Indian Institute of Technology Kanpur, Kanpur 208016 Uttar Pradesh, India;* orcid.org/0000-0001-7897-3230

Eric J. L. McInnes − *Department of Chemistry and Photon Science Institute, The University of Manchester, Manchester M13 9PL, U.K.;* orcid.org/0000-0002-4090-7040

David Collison − *Department of Chemistry and Photon Science Institute, The University of Manchester, Manchester M13 9PL, U.K.*

Complete contact information is available at: https://pubs.acs.org/10.1021/acscatal.4c01623

Author Contributions

[‖]D.P. and V.S. contributed equally.

Notes

The authors declare no competing financial interest.

■ ACKNOWLEDGMENTS

M.S. wishes to acknowledge the funding agencies SERB (CRG/2023/002178; SPR/2019/001145), CSIR (01(2933)/18/EMR-II), BRNS (58/14-2023-BRNS-37029), IISc-STARs (MoE-STARS/STARS-2/2023-0158), and RIFC, EPR central facility, IIT Bombay for the financial support. The authors are grateful to the EPSRC for funding of the EPR National Facility at Manchester (EP/V035231/1 and EP/W014521/1) and M.S. thanks the University of Manchester for financial support. A.D. likes to acknowledge SERB (SERB (CRG/2023/001112)) for the generous funding support. A.D. is thankful to SERB (CRG/2019/003058) for the financial support. G.R. would like to thank SERB for funding (SB/SJF/2019-20/12; CRG/2022/001697). V.S. thanks the PMRF for the graduate fellowship. S.S. thanks UGC for fellowship.

■ DEDICATION

Dedicated to Prof. G. K. Lahiri, IIT Bombay on the occassion of his 65th Birthday.

■ REFERENCES

(1) Dahl, S.; Chorkendorff, I. Towards practical implementation. *Nat. Mater.* **2012**, *11* (2), 100−101.

(2) Alstrum-Acevedo, J. H.; Brennaman, M. K.; Meyer, T. J. Chemical approaches to artificial photosynthesis. 2. *Inorg. Chem.* **2005**, *44* (20), 6802−6827.

(3) Sun, L.; Hammarström, L.; Åkermark, B.; Styring, S. Towards artificial photosynthesis: ruthenium−manganese chemistry for energy production. *Chem. Soc. Rev.* **2001**, *30* (1), 36−49.

(4) Gust, D.; Moore, T. A.; Moore, A. L. Solar Fuels via Artificial Photosynthesis. *Acc. Chem. Res.* **2009**, *42* (12), 1890−1898.

(5) Sala, X.; Romero, I.; Rodríguez, M.; Escriche, L.; Llobet, A. Molecular catalysts that oxidize water to dioxygen. *Angew. Chem., Int. Ed. Engl.* **2009**, *48* (16), 2842−2852.

(6) Chronister, C. W.; Binstead, R. A.; Ni, J.; Meyer, T. J. Mechanism of water oxidation catalyzed by the μ-oxo dimer $[(bpy)_2(OH_2)Ru^{III}ORu^{III}(OH_2)(bpy)_2]^{4+}$. *Inorg. Chem.* **1997**, *36* (18), 3814−3815.

(7) Binstead, R. A.; Chronister, C. W.; Ni, J.; Hartshorn, C. M.; Meyer, T. J. Mechanism of water oxidation by the μ-oxo dimer $[(bpy)_2(H_2O)Ru^{III}ORu^{III}(OH_2)(bpy)_2]^{4+}$. *J. Am. Chem. Soc.* **2000**, *122* (35), 8464−8473.

(8) Liu, F.; Concepcion, J. J.; Jurss, J. W.; Cardolaccia, T.; Templeton, J. L.; Meyer, T. J. Mechanisms of water oxidation from the blue dimer to photosystem II. *Inorg. Chem.* **2008**, *47* (6), 1727−1752.

(9) Concepcion, J. J.; Jurss, J. W.; Templeton, J. L.; Meyer, T. J. Mediator-assisted water oxidation by the ruthenium "blue dimer" cis,cis-$[(bpy)_2(H_2O)RuORu(OH_2)(bpy)_2]^{4+}$. *Proc. Natl. Acad. Sci. U.S.A.* **2008**, *105* (46), 17632−17635.

(10) Jurss, J. W.; Concepcion, J. C.; Norris, M. R.; Templeton, J. L.; Meyer, T. J. Surface catalysis of water oxidation by the blue ruthenium dimer. *Inorg. Chem.* **2010**, *49* (9), 3980−3982.

(11) Karunadasa, H. I.; Chang, C. J.; Long, J. R. A molecular molybdenum-oxo catalyst for generating hydrogen from water. *Nature* **2010**, *464* (7293), 1329−1333.

(12) Sundstrom, E. J.; Yang, X.; Thoi, V. S.; Karunadasa, H. I.; Chang, C. J.; Long, J. R.; Head-Gordon, M. Computational and Experimental Study of the Mechanism of Hydrogen Generation from Water by a Molecular Molybdenum-Oxo Electrocatalyst. *J. Am. Chem. Soc.* **2012**, *134* (11), 5233−5242.

(13) Ali, A.; Prakash, D.; Majumder, P.; Ghosh, S.; Dutta, A. Flexible Ligand in a Molecular Cu Electrocatalyst Unfurls Bidirectional O_2/H_2O Conversion in Water. *ACS Catal.* **2021**, *11* (10), 5934−5941.

(14) Nyhlén, J.; Duan, L.; Åkermark, B.; Sun, L.; Privalov, T. Evolution of O_2 in a Seven-Coordinate Ru^{IV} Dimer Complex with a $[HOHOH]^-$ Bridge: A Computational Study. *Angew. Chem., Int. Ed.* **2010**, *49* (10), 1773−1777.

(15) Grotjahn, D. B.; Brown, D. B.; Martin, J. K.; Marelius, D. C.; Abadjian, M.-C.; Tran, H. N.; Kalyuzhny, G.; Vecchio, K. S.; Specht, Z. G.; Cortes-Llamas, S. A.; et al. Evolution of iridium-based molecular catalysts during water oxidation with ceric ammonium nitrate. *J. Am. Chem. Soc.* **2011**, *133* (47), 19024−19027.

(16) Concepcion, J. J.; Jurss, J. W.; Templeton, J. L.; Meyer, T. J. One site is enough. Catalytic water oxidation by $[Ru(tpy)(bpm)(OH_2)]^{2+}$ and $[Ru(tpy)(bpz)(OH_2)]^{2+}$. *J. Am. Chem. Soc.* **2008**, *130* (49), 16462−16463.

(17) Chen, Z.; Concepcion, J. J.; Hu, X.; Yang, W.; Hoertz, P. G.; Meyer, T. J. Concerted O atom−proton transfer in the O—O bond forming step in water oxidation. *Proc. Natl. Acad. Sci. U.S.A.* **2010**, *107* (16), 7225−7229.

(18) Tseng, H.-W.; Zong, R.; Muckerman, J. T.; Thummel, R. Mononuclear ruthenium (II) complexes that catalyze water oxidation. *Inorg. Chem.* **2008**, *47* (24), 11763−11773.

(19) Zhang, G.; Zong, R.; Tseng, H.-W.; Thummel, R. P. Ru (II) Complexes of Tetradentate Ligands Related to 2, 9-Di (pyrid-2'-yl)-1, 10-phenanthroline. *Inorg. Chem.* **2008**, *47* (3), 990−998.

(20) Tong, L.; Duan, L.; Xu, Y.; Privalov, T.; Sun, L. Structural modifications of mononuclear ruthenium complexes: a combined

experimental and theoretical study on the kinetics of ruthenium-catalyzed water oxidation. *Angew. Chem., Int. Ed.* **2011**, *50* (2), 445−449.
(21) Duan, L.; Xu, Y.; Gorlov, M.; Tong, L.; Andersson, S.; Sun, L. Chemical and photochemical water oxidation catalyzed by mononuclear ruthenium complexes with a negatively charged tridentate ligand. *Chem.—Eur. J.* **2010**, *16* (15), 4659−4668.
(22) Li, L.; Duan, L.; Xu, Y.; Gorlov, M.; Hagfeldt, A.; Sun, L. A photoelectrochemical device for visible light driven water splitting by a molecular ruthenium catalyst assembled on dye-sensitized nanostructured TiO_2. *Chem. Commun.* **2010**, *46* (39), 7307−7309.
(23) Roeser, S.; Farràs, P.; Bozoglian, F.; Martínez-Belmonte, M.; Benet-Buchholz, J.; Llobet, A. Chemical, electrochemical, and photochemical catalytic oxidation of water to dioxygen with mononuclear ruthenium complexes. *ChemSusChem* **2011**, *4* (2), 197−207.
(24) Geselowitz, D.; Meyer, T. J. Water oxidation by. mu.-oxobis [bis (bipyridine) oxoruthenium (V)](4+). An oxygen-labeling study. *Inorg. Chem.* **1990**, *29* (19), 3894−3896.
(25) Hurst, J. K.; Cape, J. L.; Clark, A. E.; Das, S.; Qin, C. Mechanisms of water oxidation catalyzed by ruthenium diimine complexes. *Inorg. Chem.* **2008**, *47* (6), 1753−1764.
(26) Yamada, H.; Siems, W. F.; Koike, T.; Hurst, J. K. Mechanisms of water oxidation catalyzed by the cis, cis-$[(bpy)_2Ru(OH_2)]_2O^{4+}$ ion. *J. Am. Chem. Soc.* **2004**, *126* (31), 9786−9795.
(27) Binstead, R. A.; Moyer, B. A.; Samuels, G. J.; Meyer, T. J. Proton-coupled electron transfer between $[Ru(bpy)_2(py)OH_2]^{2+}$ and $[Ru(bpy)_2(py)O]^{2+}$. A solvent isotope effect (k_{H2O}/k_{D2O}) of 16.1. *J. Am. Chem. Soc.* **1981**, *103* (10), 2897−2899.
(28) Gersten, S. W.; Samuels, G. J.; Meyer, T. J. Catalytic oxidation of water by an oxo-bridged ruthenium dimer. *J. Am. Chem. Soc.* **1982**, *104* (14), 4029−4030.
(29) Masllorens, E.; Rodríguez, M.; Romero, I.; Roglans, A.; Parella, T.; Benet-Buchholz, J.; Poyatos, M.; Llobet, A. Can the Disproportion of Oxidation State III Be Favored in $Ru^{II}-OH_2/Ru^{IV}O$ Systems? *J. Am. Chem. Soc.* **2006**, *128* (16), 5306−5307.
(30) Yang, X.; Baik, M.-H. cis,cis-$[(bpy)_2Ru^{V}O]_2O^{4+}$ Catalyzes Water Oxidation Formally via in Situ Generation of Radicaloid $Ru^{IV}-O$. *J. Am. Chem. Soc.* **2006**, *128* (23), 7476−7485.
(31) Masaoka, S.; Sakai, K. Clear Evidence Showing the Robustness of a Highly Active Oxygen-evolving Mononuclear Ruthenium Complex with an Aqua Ligand. *Chem. Lett.* **2009**, *38* (2), 182−183.
(32) Wang, L.; Duan, L.; Stewart, B.; Pu, M.; Liu, J.; Privalov, T.; Sun, L. Toward Controlling Water Oxidation Catalysis: Tunable Activity of Ruthenium Complexes with Axial Imidazole/DMSO Ligands. *J. Am. Chem. Soc.* **2012**, *134* (45), 18868−18880.
(33) Shaffer, D. W.; Xie, Y.; Szalda, D. J.; Concepcion, J. J. Manipulating the Rate-Limiting Step in Water Oxidation Catalysis by Ruthenium Bipyridine−Dicarboxylate Complexes. *Inorg. Chem.* **2016**, *55* (22), 12024−12035.
(34) Richmond, C. J.; Matheu, R.; Poater, A.; Falivene, L.; Benet-Buchholz, J.; Sala, X.; Cavallo, L.; Llobet, A. Supramolecular Water Oxidation with Ru−bda-Based Catalysts. *Chem. - Eur. J.* **2014**, *20* (52), 17282−17286.
(35) Shaffer, D. W.; Xie, Y.; Concepcion, J. J. O−O bond formation in ruthenium-catalyzed water oxidation: single-site nucleophilic attack vs. O−O radical coupling. *Chem. Soc. Rev.* **2017**, *46* (20), 6170−6193.
(36) Wasylenko, D. J.; Ganesamoorthy, C.; Henderson, M. A.; Koivisto, B. D.; Osthoff, H. D.; Berlinguette, C. P. Electronic Modification of the $[Ru^{II}(tpy)(bpy)(OH_2)]^{2+}$ Scaffold: Effects on Catalytic Water Oxidation. *J. Am. Chem. Soc.* **2010**, *132* (45), 16094−16106.
(37) Najafpour, M. M.; Renger, G.; Hołyńska, M.; Moghaddam, A. N.; Aro, E.-M.; Carpentier, R.; Nishihara, H.; Eaton-Rye, J. J.; Shen, J.-R.; Allakhverdiev, S. I. Manganese compounds as water-oxidizing catalysts: from the natural water-oxidizing complex to nanosized manganese oxide structures. *Chem. Rev.* **2016**, *116* (5), 2886−2936.
(38) Okamura, M.; Kondo, M.; Kuga, R.; Kurashige, Y.; Yanai, T.; Hayami, S.; Praneeth, V. K. K.; Yoshida, M.; Yoneda, K.; Kawata, S.; et al. A pentanuclear iron catalyst designed for water oxidation. *Nature* **2016**, *530* (7591), 465−468.
(39) Gerken, J. B.; McAlpin, J. G.; Chen, J. Y. C.; Rigsby, M. L.; Casey, W. H.; Britt, R. D.; Stahl, S. S. Electrochemical water oxidation with cobalt-based electrocatalysts from pH 0−14: the thermodynamic basis for catalyst structure, stability, and activity. *J. Am. Chem. Soc.* **2011**, *133* (36), 14431−14442.
(40) Duan, L.; Fischer, A.; Xu, Y.; Sun, L. Isolated seven-coordinate Ru (IV) dimer complex with $[HOHOH]^-$ bridging ligand as an intermediate for catalytic water oxidation. *J. Am. Chem. Soc.* **2009**, *131* (30), 10397−10399.
(41) Murakami, M.; Hong, D.; Suenobu, T.; Yamaguchi, S.; Ogura, T.; Fukuzumi, S. Catalytic Mechanism of Water Oxidation with Single-Site Ruthenium−Heteropolytungstate Complexes. *J. Am. Chem. Soc.* **2011**, *133* (30), 11605−11613.
(42) Moonshiram, D.; Jurss, J. W.; Concepcion, J. J.; Zakharova, T.; Alperovich, I.; Meyer, T. J.; Pushkar, Y. Structure and Electronic Configurations of the Intermediates of Water Oxidation in Blue Ruthenium Dimer Catalysis. *J. Am. Chem. Soc.* **2012**, *134* (10), 4625−4636.
(43) Pushkar, Y.; Moonshiram, D.; Purohit, V.; Yan, L.; Alperovich, I. Spectroscopic Analysis of Catalytic Water Oxidation by $[Ru^{II}(bpy)(tpy)H_2O]^{2+}$ Suggests That Ru^{V}=O Is Not a Rate-Limiting Intermediate. *J. Am. Chem. Soc.* **2014**, *136* (34), 11938−11945.
(44) Lebedev, D.; Pineda-Galvan, Y.; Tokimaru, Y.; Fedorov, A.; Kaeffer, N.; Copéret, C.; Pushkar, Y. The Key RuV = O Intermediate of Site-Isolated Mononuclear Water Oxidation Catalyst Detected by in Situ X-ray Absorption Spectroscopy. *J. Am. Chem. Soc.* **2018**, *140* (1), 451−458.
(45) Amtawong, J.; Balcells, D.; Wilcoxen, J.; Handford, R. C.; Biggins, N.; Nguyen, A. I.; Britt, R. D.; Tilley, T. D. Isolation and Study of Ruthenium−Cobalt Oxo Cubanes Bearing a High-Valent, Terminal RuV−Oxo with Significant Oxyl Radical Character. *J. Am. Chem. Soc.* **2019**, *141* (50), 19859−19869.
(46) Keidel, A.; López, I.; Staffa, J.; Kuhlmann, U.; Bozoglian, F.; Gimbert-Suriñach, C.; Benet-Buchholz, J.; Hildebrandt, P.; Llobet, A. Electrochemical and Resonance Raman Spectroscopic Studies of Water-Oxidizing Ruthenium Terpyridyl−Bipyridyl Complexes. *ChemSusChem* **2017**, *10* (3), 551−561.
(47) Chen, Q.-F.; Zhang, X.; Shi, J.; Zhan, J.; Xie, F.; Zhang, H.-T.; Deng, J.; Liu, J.; Li, M.; Shao, Y.; Zhang, M.-T. In Situ Revelation of the Dynamic Evolution of Molecular Water Oxidation Catalysts. *CCS Chem.* **2024**, 1−12.
(48) Casadevall, C.; Martin-Diaconescu, V.; Browne, W. R.; Fernández, S.; Franco, F.; Cabello, N.; Benet-Buchholz, J.; Lassalle-Kaiser, B.; Lloret-Fillol, J. Isolation of a Ru (IV) side-on peroxo intermediate in the water oxidation reaction. *Nat. Chem.* **2021**, *13* (8), 800−804.
(49) Duan, L.; Bozoglian, F.; Mandal, S.; Stewart, B.; Privalov, T.; Llobet, A.; Sun, L. A molecular ruthenium catalyst with water-oxidation activity comparable to that of photosystem II. *Nat. Chem.* **2012**, *4* (5), 418−423.
(50) Maji, S.; Vigara, L.; Cottone, F.; Bozoglian, F.; Benet-Buchholz, J.; Llobet, A. Ligand Geometry Directs O−O Bond-Formation Pathway in Ruthenium-Based Water Oxidation Catalyst. *Angew. Chem.* **2012**, *124* (24), 6069−6072.
(51) Wang, L.; Duan, L.; Wang, Y.; Ahlquist, M. S. G.; Sun, L. Highly efficient and robust molecular water oxidation catalysts based on ruthenium complexes. *Chem. Commun.* **2014**, *50* (85), 12947−12950.
(52) Chen, Z.; Concepcion, J. J.; Hull, J. F.; Hoertz, P. G.; Meyer, T. J. Catalytic water oxidation on derivatized nano ITO. *Dalton Trans.* **2010**, *39* (30), 6950−6952.
(53) Concepcion, J. J.; Tsai, M.-K.; Muckerman, J. T.; Meyer, T. J. Mechanism of water oxidation by single-site ruthenium complex catalysts. *J. Am. Chem. Soc.* **2010**, *132* (5), 1545−1557.
(54) Concepcion, J. J.; Jurss, J. W.; Hoertz, P. G.; Meyer, T. J. Catalytic and Surface-Electrocatalytic Water Oxidation by Redox

https://doi.org/10.1021/acscatal.4c01623
ACS Catal. 2024, 14, 11893−11904

Mediator−Catalyst Assemblies. *Angew. Chem.* **2009**, *121* (50), 9637−9640.
(55) Gilbert, J. D.; Wilkinson, G. New complexes of ruthenium(II) with triphenylphosphine and other ligands. *J. Chem. Soc. A* **1969**, 1749−1753.
(56) Sarwar, M.; Madalan, A. M.; Tiseanu, C.; Novitchi, G.; Maxim, C.; Marinescu, G.; Luneau, D.; Andruh, M. A new synthetic route towards binuclear 3d−4f complexes, using non-compartmental ligands derived from o-vanillin. Syntheses, crystal structures, magnetic and luminescent properties. *New J. Chem.* **2013**, *37* (8), 2280−2292.
(57) Man, W.-L.; Kwong, H.-K.; Lam, W. W. Y.; Xiang, J.; Wong, T.-W.; Lam, W.-H.; Wong, W.-T.; Peng, S.-M.; Lau, T.-C. General Synthesis of (Salen)ruthenium(III) Complexes via N···N Coupling of (Salen)ruthenium(VI) Nitrides. *Inorg. Chem.* **2008**, *47* (13), 5936−5944.
(58) Chen, Z.; Concepcion, J. J.; Jurss, J. W.; Meyer, T. J. Single-site, catalytic water oxidation on oxide surfaces. *J. Am. Chem. Soc.* **2009**, *131* (43), 15580−15581.
(59) Tong, L.; Wang, Y.; Duan, L.; Xu, Y.; Cheng, X.; Fischer, A.; Ahlquist, M. S. G.; Sun, L. Water oxidation catalysis: influence of anionic ligands upon the redox properties and catalytic performance of mononuclear ruthenium complexes. *Inorg. Chem.* **2012**, *51* (6), 3388−3398.
(60) Matheu, R.; Ertem, M. Z.; Gimbert-Suriñach, C.; Sala, X.; Llobet, A. Seven coordinated molecular ruthenium−water oxidation catalysts: a coordination chemistry journey: focus review. *Chem. Rev.* **2019**, *119* (6), 3453−3471.
(61) Ghaderian, A.; Franke, A.; Gil-Sepulcre, M.; Benet-Buchholz, J.; Llobet, A.; Ivanović-Burmazović, I.; Gimbert-Suriñach, C. A broad view on the complexity involved in water oxidation catalysis based on Ru−bpn complexes. *Dalton Trans.* **2020**, *49* (47), 17375−17387.
(62) Costentin, C.; Drouet, S.; Robert, M.; Savéant, J. M. Correction to Turnover Numbers, Turnover Frequencies, and Overpotential in Molecular Catalysis of Electrochemical Reactions. Cyclic Voltammetry and Preparative-Scale Electrolysis. *J. Am. Chem. Soc.* **2012**, *134* (48), 19949−19950.
(63) Matheu, R.; Neudeck, S.; Meyer, F.; Sala, X.; Llobet, A. Foot of the Wave Analysis for Mechanistic Elucidation and Benchmarking Applications in Molecular Water Oxidation Catalysis. *ChemSusChem* **2016**, *9* (23), 3361−3369.
(64) Shatskiy, A.; Bardin, A. A.; Oschmann, M.; Matheu, R.; Benet-Buchholz, J.; Eriksson, L.; Kärkäs, M. D.; Johnston, E. V.; Gimbert-Suriñach, C.; Llobet, A.; Åkermark, B. Electrochemically Driven Water Oxidation by a Highly Active Ruthenium-Based Catalyst. *ChemSusChem* **2019**, *12* (10), 2251−2262.
(65) Wu, Y.; Klein, V.; Killian, M. S.; Behling, C.; Chea, S.; Tsogoeva, S. B.; Bachmann, J. Novel fully organic water oxidation electrocatalysts: A quest for simplicity. *ACS Omega* **2018**, *3* (3), 2602−2608.
(66) Blakemore, J. D.; Crabtree, R. H.; Brudvig, G. W. Molecular catalysts for water oxidation. *Chem. Rev.* **2015**, *115* (23), 12974−13005.
(67) Murray, K. S.; Van, d. B. A. M.; West, B. O. Ruthenium complexes with a tetradentate salicylaldimine Schiff base. *Aust. J. Chem.* **1978**, *31* (1), 203−207.
(68) Cape, J. L.; Lymar, S. V.; Lightbody, T.; Hurst, J. K. Characterization of Intermediary Redox States of the Water Oxidation Catalyst, $[Ru(bpy)_2(OH_2)]_2O^{4+}$. *Inorg. Chem.* **2009**, *48* (10), 4400−4410.
(69) Bystron, T.; Horbenko, A.; Syslova, K.; Hii, K. K.; Hellgardt, K.; Kelsall, G. 2-Iodoxybenzoic Acid Synthesis by Oxidation of 2-Iodobenzoic Acid at a Boron-Doped Diamond Anode. *ChemElectroChem* **2018**, *5* (7), 1002−1005.
(70) Bystron, T.; Devadas, B.; Bouzek, K.; Svoboda, J.; Kolarikova, V.; Kvicala, J. Anodic Oxidation of Iodobenzene and Iodobenzoic Acids in Acetic Acid Environment − Electrochemical Investigation and Density Functional Theory Study. *ChemElectroChem* **2021**, *8* (19), 3755−3761.
(71) Polyansky, D. E.; Muckerman, J. T.; Rochford, J.; Zong, R.; Thummel, R. P.; Fujita, E. Water Oxidation by a Mononuclear Ruthenium Catalyst: Characterization of the Intermediates. *J. Am. Chem. Soc.* **2011**, *133* (37), 14649−14665.
(72) Yamada, H.; Hurst, J. K.; Resonance, R. Resonance Raman, Optical Spectroscopic, and EPR Characterization of the Higher Oxidation States of the Water Oxidation Catalyst, *cis*,*cis*-$[(bpy)_2Ru(OH_2)]_2O^{4+}$. *J. Am. Chem. Soc.* **2000**, *122* (22), 5303−5311.
(73) Shi, J.; Guo, Y. H.; Xie, F.; Chen, Q. F.; Zhang, M. T. Redox-Active Ligand Assisted Catalytic Water Oxidation by a RuIV= O Intermediate. *Angew. Chem.* **2020**, *132* (10), 4029−4037.
(74) Ishizuka, T.; Kotani, H.; Kojima, T. Characteristics and reactivity of ruthenium−oxo complexes. *Dalton Trans.* **2016**, *45* (42), 16727−16750.
(75) Kojima, T.; Nakayama, K.; Ikemura, K.; Ogura, T.; Fukuzumi, S. Formation of a ruthenium (iv)-oxo complex by electron-transfer oxidation of a coordinatively saturated ruthenium (II) complex and detection of oxygen-rebound intermediates in C−H bond oxygenation. *J. Am. Chem. Soc.* **2011**, *133* (30), 11692−11700.
(76) Concepcion, J. J.; Jurss, J. W.; Norris, M. R.; Chen, Z.; Templeton, J. L.; Meyer, T. J. Catalytic water oxidation by single-site ruthenium catalysts. *Inorg. Chem.* **2010**, *49* (4), 1277−1279.
(77) Chen, Z.; Concepcion, J. J.; Luo, H.; Hull, J. F.; Paul, A.; Meyer, T. J. Nonaqueous catalytic water oxidation. *J. Am. Chem. Soc.* **2010**, *132* (50), 17670−17673.

https://doi.org/10.1021/acscatal.4c01623
ACS Catal. 2024, 14, 11893−11904